Karya#5 Plagiasi

by Marjoni Imamora

Submission date: 07-Jun-2020 11:41AM (UTC+0700)
Submission ID: 1339170101
File name: Karya_5_Q1_Penulis_Bersama.pdf (3.55M)
Word count: 8266
Character count: 42672

ACS OMEGA

Article

Cite This: ACS Omega 2018, 3, 2579−2587

Two-Dimensional, Hierarchical Ag-Doped TiO_2 Nanocatalysts: Effect of the Metal Oxidation State on the Photocatalytic Properties

Siti Khatijah Md Saad,[†] Akrajas Ali Umar,*[,†] Marjoni Imamora Ali Umar,[‡] Masahiko Tomitori,[§] Mohd. Yusri Abd. Rahman,[†] Muhamad Mat Salleh,[†] and Munetaka Oyama[∥]

[†]Institute of Microengineering and Nanoelectronics, Universiti Kebangsaan Malaysia, 43600 Bangi, Selangor, Malaysia

[‡]Department of Physics Education, Faculty of Tarbiyah, Institut Agama Islam Negeri (IAIN), Batusangkar, 27213 West Sumatra, Indonesia

[§]School of Materials Science, Japan Advanced Institute of Science and Technology, 1-1 Asahidai, Nomi, Ishikawa 923-1292, Japan

[∥]Nanomaterials Chemistry Laboratory, Department of Materials Chemistry, Graduate School of Engineering, Kyoto University, Nishikyo-ku, Kyoto 615-8520 Japan

Supporting Information

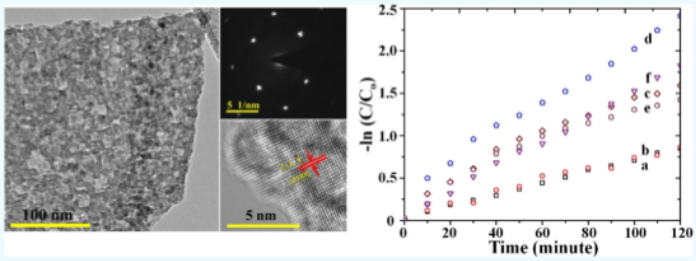

ABSTRACT: This paper reports the synthesis of two-dimensional, hierarchical, porous, and (001)-faceted metal (Ag, Zn, and Al)-doped TiO_2 nanostructures (TNSs) and the study of their photocatalytic activity. Two-dimensional metal-doped TNSs were synthesized using the hydrolysis of ammonium hexafluorotitanate in the presence of hexamethylenetetramine and metal precursors. Typical morphology of metal-doped TNSs is a hierarchical nanosheet that is composed of randomly stacked nanocubes (dimensions of up to 5 μm and 200 nm in edge length and thickness, respectively) and has dominant (001) facets exposed. Raman analysis and X-ray photoelectron spectroscopy results indicated that the Ag doping, compared to Zn and Al, much improves the crystallinity degree and at the same time dramatically lowers the valence state binding energy of the TNS and provides an additional dopant oxidation state into the system for an enhanced electron-transfer process and surface reaction. These are assumed to enhance the photocatalytic of the TNS. In a model of photocatalytic reaction, that is, rhodamine B degradation, the AgTNS demonstrates a high photocatalytic activity by converting approximately 91% of rhodamine B within only 120 min, equivalent to a rate constant of 0.018 m^{-1} and ToN and ToF of 94 and 1.57 min^{-1}, respectively, or 91.1 mmol mg^{-1} W^{-1} degradation when normalized to used light source intensity, which is approximately 2 times higher than the pristine TNS and several order higher when compared to Zn- and Al-doped TNSs. Improvement of the crystallinity degree, decrease in the defect density and the photogenerated electron and hole recombination, and increase of the oxygen vacancy in the AgTNS are found to be the key factors for the enhancement of the photocatalytic properties. This work provides a straightforward strategy for the preparation of high-energy (001) faceted, two-dimensional, hierarchical, and porous Ag-doped TNSs for potential use in photocatalysis and photoelectrochemical application.

INTRODUCTION

Morphology, atomic stoichiometry, and surface physicochemical properties of catalyst systems determine the photocatalytic activity, charge transfer, and other surface reactions.[1−7] Catalysts with morphology containing high-energy facets and wide surface areas are highly demanded as they could generate excellent photochemical activity. For the anatase TiO_2 nanocatalyst, the (001) facet is the highest energy facet with an outstanding stability and is the second in the surface energy among the lowest-index planes following an order of (110) > (001) > (100) > (101) with their corresponding surface energy of 1.09, 0.90, 0.53, and 0.44 J m^{-2}, respectively.[8] In addition, because the nanocatalyst has unique Ti and O atoms arrangements, with the Ti−O bond being relatively longer than that in other facets, and higher density of five-coordinated Ti(001) facet surface atoms, compared to the typical surface of (101) faceted TiO_2, its electron distribution density is loosely bound to the atoms. This will result in abundance of energetic

Received: January 18, 2018
Accepted: February 20, 2018
Published: March 5, 2018

   DOI: 10.1021/acsomega.8b00109
ACS Omega 2018, 3, 2579−2587

electrons that may be available for charge-transfer activity and surface reactions. Various fields of applications, such as photocatalysts, photovoltaics, photoelectrochemical cell applications, hydrogen generation, water splitting, and so forth, have been reported to be multiplied in efficiency when utilizing the (001)-faceted TiO_2 nanomaterial.[9−14] Therefore, any efforts should be continuously demonstrated to realize the anatase TiO_2 nanocatalyst with the wide-area (001) facet.

The efforts of synthesizing TiO_2 with (001) facets has started since 2008 as reported by the Yang research group.[15] To date, a wide range of approaches for the synthesis of anatase TiO_2 with such characteristics have been available with most of them being centered on using of the fluorination effect in projecting the (001) facet in the TiO_2 nanostructure (TNS).[16−19] For example, the hydrothermal technique involving the addition of hydroflouric acid into the TiO_2 precursor, such as $TiCl_4$, has successfully produced (001)-faceted solid surface TiO_2 with a lateral size of up to 1 μm.[20] The solvothermal technique for decomposing $TiOF_2$ in the presence of tetrabutyl titanate, hydroflouric acid, and acetic acid was found to be capable of producing hollow box TiO_2 with an edge length of 500 nm.[21] Still, there are several methods opting not to include the presence of hydroflouric acid during the reaction, such as reported by Cheng et al., where by decomposing the titanium butoxide in the presence of concentrated hydrochloric acid, solid TiO_2 nanosheets with an edge length as high as 200 nm can be obtained.[22] Even though such reported techniques have successfully realized (001) faceted TiO_2, the samples were mostly characterized by solid structures and wider dimensions, that is, in the range of 100 nm up to micrometers in size.[23,24] With such solid structure characteristics and bulklike dimensions, the surface area could be low and the unique properties resulting from the quantum effect would also be unavailable in nanostructures with such micrometer dimensions. Therefore, preparation of TNSs with higher surface areas but maintaining their quantum characteristics, such as wide-area and ultra-thin nanosheets, has been highly demanded.

In an earlier study, we found that the porous anatase TiO_2 nanoplates that were grown vertically on a substrate surface resembling a nanowall structure[25] exhibited excellent photocatalytic properties in the photodegradation of methylene blue. The photocatalytic performance becomes extremely enhanced when the nanoplate was doped with Zn. Here, we report the synthesis of porous, two-dimensional (2D), hierarchical TNSs and the study of the role of metal doping of different oxidation states in their photocatalytic properties. It has been well-known that the oxidation state of a metal dopant has a profound effect on the modification of the electron density of state via electron donating and accepting with the dopant, improving the oxygen vacancy and refinement of crystallinity in the metal oxides nanocrystals, as well as reducing the electron−hole recombination or facilitating a facile electron−hole separation that is useful for promoting the active electron-transfer process for the highly efficient photocatalytic process.[26−30] In addition, the unique optical properties of metal nanoparticles, such as localized surface plasmon resonance, acoustogyration, and nonlinear optical effects, are expected to intensely modify the optical properties of the metal-oxide nanocrystals when being doped with them.[31−36] In this work, we achieved a high photocatalytic performance in a rhodamine B degradation by using the Ag-doped TNS (AgTNS), which is several order higher compared to the TNS doped with Zn or Al. In the typical process, the AgTNS can degrade rhodamine B up to 91% within only 120 min, which is equivalent to ToN and ToF of 94 and 1.57 min^{-1}, respectively. An expanded crystallinity refinement in the TNS nanocrystal lattice, which at the same time dramatically lowers the valence state binding energy of TNS and provides the additional dopant oxidation state into the system for enhanced electron-transfer process and surface reaction, is assumed as the key factor for the high photocatalytic performance in the AgTNS system. The synthetic process and the photocatalytic performance of metal-doped TNSs will be discussed.

RESULTS AND DISCUSSION

AgTNS Characterization. During the growth process of the AgTNS, the initial solution is colorless. The solution immediately shows a greyish color with time elapsing. At 5 h of growth time, the solution becomes colorless and greyish-white precipitates were obtained. The morphology and the structure of the sample were then analyzed using field emission scanning electron microscopy (FESEM) and high-resolution transmission electron microscopy (HRTEM). Figure 1 shows the characteristic of the AgTNS morphology prepared using a reaction containing 5 mL of 0.5 ammonium hexafluorotitanate, 1 mL of 0.5 hexamethylenetetramine (HMT), and 1 mL of 100 mM $AgNO_3$. As can be seen in Figure 1, the morphology of the samples is a square-shaped nanosheet with an edge length and a thickness of up to 5 μm and 200 nm, respectively. As also can be seen in the Figure 1A−C, the nanosheet exhibits a porous hierarchical structure in nature, which is composed of oriented stacking of small nanocuboids of TiO_2 of dimensions approximately 50 and 100 nm in length and width, which is similar to the structure of the TiO_2 nanowall that has been previously reported.[25] However, here we found that the AgTNS is much porous, brittle, and thinner. This is probably due to the existence of an unique combinative effect of Ag and nitric ions from $AgNO_3$ salt in the reaction, which is well-known as a strong reducing agent that may induce surface oxidation or Ostwald annealing, generating thinner nanosheet structures. It is also assumed that both Ag and nitric ions may play adhesive role so that the wide open pore structure of nanocuboid stacking can be possibly retained. Using different nitric salts, such as zinc nitrate, aluminum nitrate, and so forth, may not produce such a thin and porous nanosheet structure.

To obtain the crystallinity of the nanosheets, we carried out HRTEM analysis. The results are shown in Figure 1D−F. To our surprise, despite the nanosheet nanostructures being composed of stacked nanocuboids, it is found that the nanosheets are single crystalline in nature because of the presence of clear lattice fringes without twinning and dislocation. Such a single crystalline nature is further verified by the selected-area electron diffraction (SAED) analysis results. We calculated the lattice spacing and it was found to be 0.24 nm, which belongs to the (001) facet of anatase TiO_2. SAED also confirmed the nature of the (001) facet because of the presence of a square-shaped electron diffraction pattern (see Figure 1E).

Because of the existence of Ag ions in the reaction, the AgTNS is expected to be reproduced as confirmed by X-ray powder diffraction (XRD), energy-dispersive X-ray spectroscopy (EDX), and X-ray photoelectron spectroscopy (XPS) analysis, which will be discussed later. Nevertheless, interestingly, judging from the high-resolution FESEM image, no nanostructures related to Ag are observed on the nanosheet reflecting that the Ag doping follow the substitutional doping

DOI: 10.1021/acsomega.8b00109
ACS Omega 2018, 3, 2579−2587

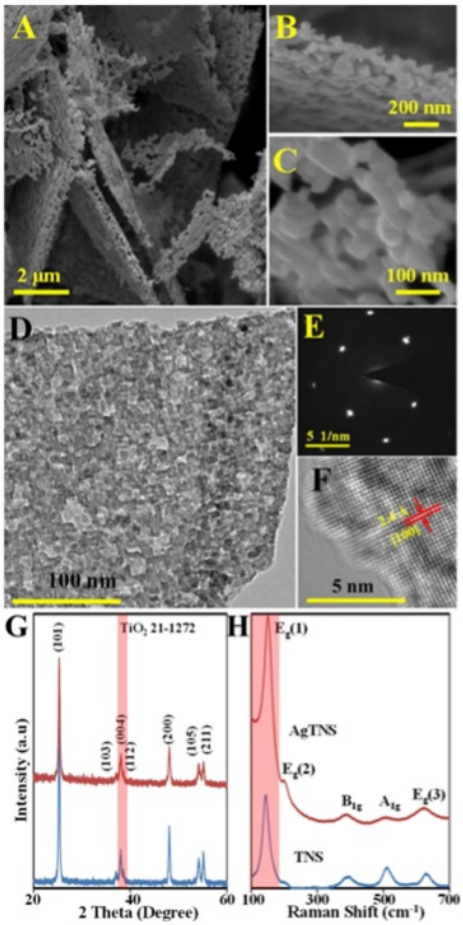

Figure 1. Morphological and phase crystallinity characterization result for AgTNS samples. (A–C) Low- and high-resolution images showing the hierarchical structure of the nanosheet that is composed of stacked-small nanocuboid of TiO_2. (D–F) Low- and high-resolution image as well as SAED spectrum of AgTNS samples. (G,F) XRD and Raman spectra of AgTNS samples and their comparison with spectra of the pristine TNS, which show significant shifting in the main peaks indicating effective modification of structure upon being doped with Ag. Shaded area in G and H highlighting the shifting of the main peaks of XRD and Raman spectra.

process. However, at high concentration Ag doping, for example, 150 and 200 mM, Ag nanoparticles are visible on the surface of the nanosheet (Figure S1, Supporting Information). This could be due to the supersaturation of doping of Ag onto the TiO_2 nanosheet lattice.

To confirm the phase crystallinity of the as-synthesized nanosheets, we carried out XRD spectroscopy analysis. Figure 1G shows the corresponding XRD spectrum for the sample. XRD samples followed the standard XRD pattern for anatase TiO_2 (JCPDS file number 21-1272). The main peaks of anatase TiO_2 are observed at 25.28, 36.50, 37.80, 38.58, 48.05, 53.89, and 55.06°, which are associated with the lattice planes of (101), (103), (004), (112), (200), (105), and (211), respectively. Surprisingly, no peaks related to fcc Ag crystal are observed in this spectrum, inferring that Ag ions successfully substituted into the anatase TiO_2 lattice. The doping process on the TNS is likely confirmed by the existence of shifting in the main peaks toward a higher angle, reflecting an effective stressing in the TNS lattice upon the Ag-ion substitution. The shifting increases with the increasing Ag doping concentration and is optimum at the TNS sample doped with 100 mM of Ag doping (Figure S2, Supporting Information). The Raman analysis result also further validates the successfulness of the Ag doping into the TNS. As can be seen from the Raman spectrum in Figure 1H, there has been a shifting in the position of the main Raman peaks for TiO_2, that is, Eg(1), Eg(2), and B_{1g} mode (the peak related to bridge oscillation of O–Ti–O bending) and Eg(3) and A_{1g} (Ti–O strain oscillation), to the higher frequency upon doping with the Ag.[37−39] This indicates that the Ag doping effectively distorts the stoichiometry of the lattice chemical composition and enhances the surface oxidation state due to the improvement of the oxygen vacancy density and the decrease in the recombination of photogenerated electrons and holes.[40] These results reveal that the Ag doping should enhance the surface reactivity of the TNS. Similar to the XRD result, the shifting increase with the increasing Ag doping content (Figure S3, Supporting Information). Additional verification on the doping process has also been carried via elemental analysis using the EDX technique. The result is shown in Figure S4 (Supporting Information). As can be seen in the figure, the Ag element along with the TiO_2 component with the atomic concentration approximately 0.3% is observed in the spectrum. Elemental mapping composition on the sample further indicates that the Ag element is homogenously distributed throughout the nanocrystal (Figure S4). Nevertheless, at lower Ag concentrations, that is, 25–50 mM, the Ag element cannot be detected presumably because of the low percentage of Ag ion in the TNS lattice. However, Raman spectra as shown in Figure S3 show a significant shifting in the Eg bands toward higher frequency, indicating a lattice symmetry modification of which is associated with the Ag doping.[40] In addition, from the EDX elemental analysis as shown in Table 1, there has been a decrease in the impurity content, particularly the F element,

Table 1. Optical Properties and Photocatalytic Performance of the AgTNS

	element (wt %)					photocatalytic performance			
Ag^+ conc. (mM)	Ti	O	Ag	F	band gap (eV)	% Deg.	kinetic rate, K	ToN	ToF
0	28.6	60.5		10.9	3.31	57.14	0.0068	48.36	0.80
25	20.7	72.5		6.8	3.3	57.82	0.0069	50.93	0.85
50	24.2	70.5		5.2	3.28	79.68	0.012	81.62	1.36
100	24.3	74.9	0.2	5.1	3.28	91.07	0.018	93.98	1.57
150	24.2	70.5	0.3	4.9	3.25	75.94	0.011	79.03	1.32
200	20.3	74.7	0.7	4.3	3.30	83.95	0.015	74.56	1.24

DOI: 10.1021/acsomega.8b00109
ACS Omega 2018, 3, 2579−2587

when the TNS was being doped with Ag. This could only occur when different impurities share the binding sites with the F element, a strong evidence of the Ag substitution into the TNS lattice. On the basis of these analysis results, it is worthwhile remarked that the AgTNS has been successfully realized.

We then carried out XPS analysis on the sample to understand its surface chemistry properties. The results are shown in Figure 2. As can be seen from the wide-range scan

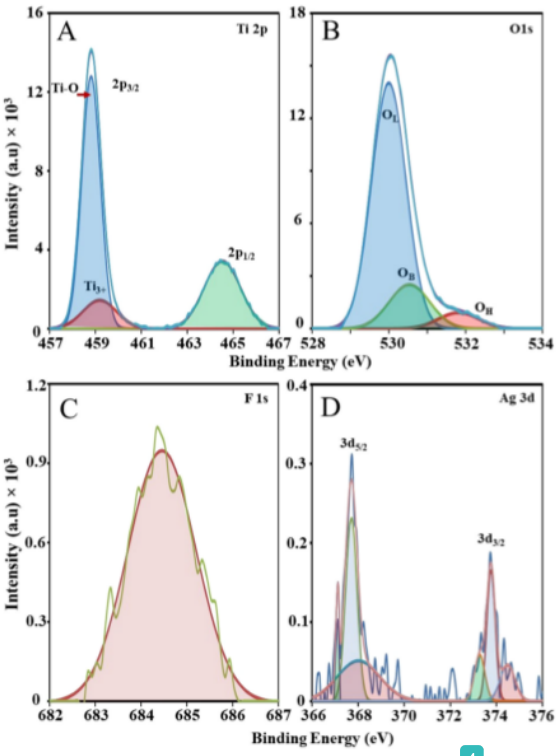

Figure 2. High-resolution XPS spectra of AgTNS samples with the Ag precursor concentration of 100 mM. (A) Ti 2p, (B) O 1s, (C) F 1s, and (D) Ag 3d spectra. Shaded region under the fitted curves reveals the percentage of the chemical state.

result in Figure S5 (Supporting Information), binding energies related to the AgTNS elements, that is, Ti, O, and Ag, are also observed along with F binding energy, which is related to surface fluorination. This result is in good agreement with the EDX elemental analysis result as shown in Figure S4. Other elements from the indium tin oxide (ITO) substrate, such as Sn and In, are also obtained. To further understand the nature of chemical bonding on the sample surface, we carried out high-resolution scan on each element. A carbon correction at 284.5 eV was performed on each high-resolution scan. For the case of the Ti element (Figure 2A), the binding energy is split into two spin orbits at the energy of 458.81 and 464.52 eV that correspond to Ti^{4+} $2p_{3/2}$ and Ti^{4+} $2p_{1/2}$, respectively. When compared to the pristine TNS samples, the Ti 2p lattice peaks actually shift to a higher binding energy. It is due to the fact that the electron density of Ti is lowered upon being doped with Ag, confirming the successful doping of Ag into the TiO_2 lattice. The decrease in the electron density in the Ti site may cause the decrease in the optical band gap energy of the TNS, which in turn enhances the photoactivity of the samples. Thus, the photocatalytic performance is expected to be improved. This high-resolution scan spectrum is well-fitted by two Gaussian (G) curves with the energy centered at 458.81 and 459.18 eV, which are associated with the lattice (Ti−O) and Ti^{3+} binding energy, respectively. The Ti^{3+} peak is mainly associated with the binding energy for impurity or doping. Thus, in this case, this peak could be due to the Ti−Ag binding energy. The area ratio is relatively high, that is, 12% (see the shaded region under the curve in Figure 2A). Nevertheless, the Ti^{3+} peaks are much higher in the pristine TNS with the area ratio as high as 15%. This is due to the nature of facile bonding of impurities, such as F and N, onto the TNS lattice. However, in the presence of Ag ions in the reaction, a better immiscibility of Ag ions in the TiO_2 lattice[41] may overcome the other impurities binding to the lattice. Because of a relatively high ionic radius of Ag, the intensity of the binding energy band related to Ti−Ag becomes lower than that of the pristine TNS samples. This has also been confirmed by the EDX elemental analysis results as shown in Table 1, which shows the decreasing atomic percentage of the F element in the EDX spectra upon the increase of the Ag doping concentration. Meanwhile, regarding the oxygen (Figure 2B), its high-resolution scanning spectrum can be well-fitted by three G curves that are centered at 529.99, 530.54, and 531.82 eV, which are attributed to lattice (O_L), bridging (O_B), and hydroxyl (O_H) species binding energies. Binding energy related to bridging can be associated with the binding energy impurities, such as Ag−O and surface fluorination, which also confirmed in the high-resolution scan of F 1s binding energy as shown in Figure 2C. Its area ratio is as high as 16.57%. Similar to the Ti impurity binding energy, the O_B area intensity in the pristine TNS sample is also higher than in the AgTNS, that is, 36.21%, which is attributed to F or N impurities chemical binding energies. For the case of Ag, similar to Ti, its high-resolution scan also consists of two spin orbit splitting with energy centered at 367.73 and 373.73 eV (see Figure 2D). It (Ag $d_{5/2}$) can be again well-fitted by three G curves that correspond to binding energy of impurities (367.09 and 367.70 eV) and lattice (368.01 eV) with area ratios of 59 and 41%, respectively. The high area ratio of binding energy related to impurities indicating the effective substitutional doping of Ag into the TNS lattice. Owing to the effective substitutional doping of Ag into the TNS lattice, it is expected that the AgTNS should have much better photocatalytic activity compared to the pristine anatase TiO_2.

The optical properties of the TNS samples (Figure 3) changed with the doping of Ag into the TNS by presenting a meaningful alteration of the optical energy gap of the TNS upon doping, that is, they decreased with the increase of the doping concentration and reached a minimum at a doping concentration of 100 mM with an optical band gap value of 3.28 eV. The optical energy band gap then increases when the doping concentration further increases above this value. The results are summarized in Table 1. It can be attributed to the doping supersaturation effect that makes the Ag interstitially grow on the surface of the TNS, as judged by the FESEM analysis in Figure S1.

Photocatalytic Characterization. The photocatalytic properties of the porous, hierarchical AgTNS was evaluated by rhodamine B (RhB) degradation under solar simulator light irradiation. Typical absorption spectra of RhB during a photocatalytic degradation over AgTNS with an Ag concentration of 100 mM is shown in Figure 4. As can be seen in the

DOI: 10.1021/acsomega.8b00109
ACS Omega 2018, 3, 2579−2587

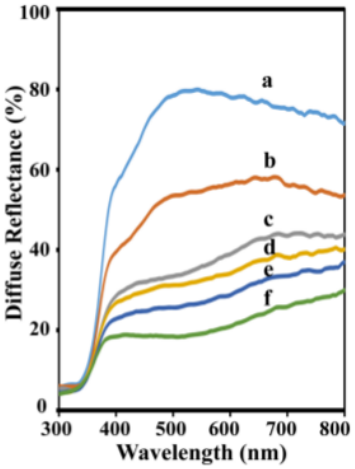

Figure 3. Diffuse reflectance spectra for TNS treated with the Ag precursor at $AgNO_3$ with six different concentrations of (a) 0, (b) 25, (c) 50, (d) 100, (e) 150, and (f) 200 mM.

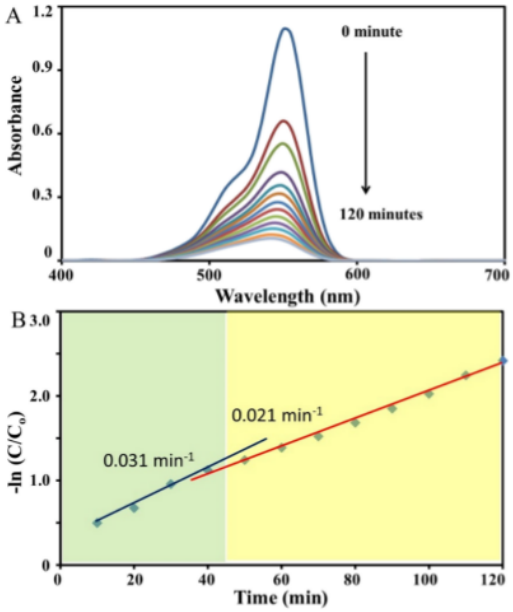

Figure 4. Photodegradation kinetics of rhodamine B over the AgTNS under irradiation of solar light simulator 100 mW cm^{-2} AM1.5. (A) Absorption spectra of rhodamine B during the photocatalytic degradation. (B) Reaction kinetic rate of the photocatalytic degradation of rhodamine B showing two regions of reaction kinetics (shaded region), that is, high- and low-kinetic conditions.

figure, the characteristic absorption band of RhB centered at 550 nm rapidly decreased with the increasing of the reaction time. From the concentration calibration curve in Figure S6 (Supporting Information), it can be understood that the RhB concentration is effectively reduced with the increasing reaction time and reduces up to 91% from 10 ppm (initial concentration) to 0.89 ppm for a reaction time of 120 min. The kinetic rate of the reaction was calculated to be as high as 0.018 min^{-1}. From the reaction kinetic plot, it is discovered that the change in the RhB concentration is in general linear with the reaction time, which follows the first-order reaction kinetics. However, it can be divided into two different reaction kinetic conditions, that is, high rate (approximately 0.031 m^{-1}) at the beginning of the reaction up to 30 min and lower rate (0.021 m^{-1}) at the longer reaction time. This could be related to the fact of active site poisoning at longer reaction time, causing a decrease in the reaction kinetic rate. Nevertheless, the difference between the high reaction rate and the lower reaction rate regions is not large, indicating that the AgTNS has a highly dynamic surface chemical process and high active site chemical stability properties. By considering the amount of AgTNS molarity used in the reaction, we then calculated the turn-over-number (ToN) and turn-over-frequency (ToF) of the reaction and the values as high as 94 and 1.57 m^{-1} were recorded for ToN and ToF, respectively. These values are several order higher compared to those of the pristine TNS sample, confirming the high photocatalytic performance of the AgTNS.

Because of the fact that the photocatalytic degradation not only depends on the molarity of the catalyst system but also on the intensity of the solar light source used during the reaction, we calculated the efficiency of the reaction by considering both the factors. We then found that the present sample demonstrated extremely high photocatalytic performance with efficiency as high as 91.1 mg^{-1} W^{-1}, which is double from that of the most recently reported result (see Table 2).

Figure 4A shows a typical plot of the reaction kinetic rate over AgTNS samples with different Ag doping concentrations during the RhB photocatalytic degradation reaction. It can be observed from the figure that the reaction kinetic rate remarkably increases upon doping and is optimum at the Ag doping concentration of 100 mM. The kinetic rate changes from 0.0069 on pristine TNS to 0.0180 min^{-1} on the optimum AgTNS sample. However, the photocatalytic performance gradually decreased when the Ag doping concentration further increased above the optimum value.

There are several factors that influence the photocatalytic properties, including the modification of surface chemistry, optical band gap, surface morphology of the samples, and so forth. In the present study, we remark that the modification of the surface chemistry and the optical properties of the samples are the main reasons for the improvement of the photocatalytic performance upon being doped with the Ag ion. Pristine TNS, because of its unique (001) faceted and hierarchical structure, readily demonstrates high photocatalytic performance in the degradation of RhB. In our current study, the kinetic rate as high as 0.0069 min^{-1} has been recorded for this pristine TNS sample. Introduction of doping has modified and enhanced the surface chemistry properties of the TNS because of the modification of lattice symmetry and the electronics system, leading to a highly active chemical reaction on their surface. According to the XPS analysis result, there has been a significant shifting toward the lower energy of the electrons in the Ti $p_{3/2}$ state upon the introduction of Ag ions into the lattice, suggesting that there has been an improvement in the reactivity nature of the surface. However, when the doping process involves an interstitial growth of Ag nanoparticles on the TNS lattice, especially at high Ag concentrations (e.g., higher than 150 mM), the photocatalytic performance reduces. This is associated with the deterioration of the surface active site by the Ag nanoparticle interstitial growth, limiting the adsorption of the RhB molecules onto the AgTNS surface and

:10.1021/acsomega.8b00109
ACS Omega 2018, 3, 2579−2587

Table 2. Comparison of Photocatalytic Performance of the AgTNS with Other TiO_2 Systems

sample	% Deg.	kinetic rate, K (min^{-1})	power (W)	efficiency[a], % Deg/W × mg	reaction time (min)	ref
AgTNS	91.1	0.0180	100	91.1	120	our data
TNS	42.9	0.0069	100	42.9	120	our data
ZnTNS	67.7	0.0092	100	67.7	120	our data
AlTNS	41.1	0.0045	100	41.1	120	our data
$Zn_xCd_{1-x}S/TiO_2$	96.0		500	38.4	120	42
NH_3TiO_2	93		350	26.6	120	43
N-TiO_2	84		84	56.0	120	44
CeO_2 doped TiO_2	93	0.00021	150	12.4	60	45
PANI/MS-TiO_2	99.8	0.0310	300	3.3	120	46
TiO_2 nanowires	98.9		800	24.73	60	47

[a]Calculation was based on 1 mg catalyst.

the surface reaction, trapping the photogenerated electron, and accordingly, affecting the photocatalytic degradation of RhB. Thus, the photocatalytic performance decreases. The presence of the Ag metal dopant in the AgTNS may also contribute to formation of much more electron trapping sites in the nanocrystal. This phenomenon may facilitate the separation of electrons and holes and assist in the electron-transfer process at the interface, promoting an active photocatalytic process. In addition, the presence of the moderately lower weight percentage of F atom in the AgTNS sample also drives energetic photocatalytic activity when compared to the pristine TNS with a high concentration of surface fluorination, which is normally obtained on (001)-faceted TiO_2 nanocrystals. The presence of F atoms in the samples causes surface poisoning, limiting the formation of $OH^{\bullet}$ radicals that is beneficial for RhB degradation. Therefore, decreasing the concentration of surface fluorination, which is achieved in the AgTNS, may lead to higher catalytic activity.

The lowering in the optical band gap of the TNS upon being doped with Ag could also be the reason for the performance improvement. It was found that the optical band gap of the TNS significantly reduced upon being doped with Ag where the optical band gap reduction increases with the increasing Ag doping concentration and reaches optimum at the AgTNS sample with the Ag precursor concentration of 100 mM (Figure S5, Supporting Information). This changes from 3.31 eV for pristine TNS to 3.28 eV for the optimum AgTNS samples. Actually, the sample that are doped with higher Ag concentrations also shows an appreciably decrease in their optical band gap. However, because of other surface chemistry effects, that is, the disruption of the surface active site by interstitial Ag nanoparticles growth (see Figure S1, Supporting Information), the sample with the high Ag doping concentration is much low in the photocatalytic performance. Although in many cases, such interstitially grown metallic nanoparticles may enhance the optical properties of the host materials via metal catalytic[48] or plasmonic effects,[32] in the present study it may behave as a trap to the photoexcited carriers, decreasing the photocatalytic performance of the AgTNS.

The modification of the morphology upon doping is also assumed to generate a profound effect on the photocatalytic performance. As has been discussed earlier, the structure becomes more porous upon being doped with Ag (see Figure S1, Supporting Information). The improvement of the AgTNS porosity enhances the surface interaction between the catalyst and the analytes. Thus, the photocatalytic degradation of RhB is improved.

It has been well-known that the electrical, optical, and surface physicochemical properties of the TiO_2 nanocrystals are also determined by the metal dopant properties, particularly its ionic radius and oxidation state.[49] The use of metals with different ionic radii and oxidation states may modify the surface chemistry of the nanostructure because of the alteration of oxygen vacancy either in bulk or surface of the anatase TiO_2, increasing the uncoordinated-species (dangling bond) density on the surface and the surface atom reconstruction. We prepared the TNS doped with Zn and Al, and their FESEM image and XRD spectra are shown in Figures S7 and S8 (Supporting Information). We compared the photocatalytic properties of AgTNS with Zn- and Al-doped TNS to understand the role of metal doping type in the photocatalytic properties of anatase TNS. We found that the AgTNS that contains Ag dopants demonstrates the highest photocatalytic efficiency and followed by Zn and Al. The results are shown in Figure 5B. It has been acclaimed that the number of oxidation states of the metal dopant may either stabilize or destabilize the host material lattice via the lattice symmetry distortion, which in turn modify the electron density of state of the host material. Similar effect is assumed to be valid for the case of ionic radii in the modification of the surface physicochemistry properties. The larger the dopant ionic size, immense the lattice symmetry distortion is, and thus, the greater the modification of the surface electronic density of state. XPS analysis result verifies such phenomena as the shifting in the chemical species state binding energy as well as the modification of the chemical states in both Ti and O (Figure 6). For example, the shifting to the higher energy in Ti chemical state binding energy is observed in the AgTNS sample, whereas to the lower binding energy for ZnTNS and AlTNS. A similar case is also observed in the O chemical state binding energy, in the O species, the binding energy related to bridging and hydroxyl chemical states also demonstrates shifting its energy to the higher energy region when the TNS doped with Ag and otherwise when being doped with Zn and Al. Different with the Ti site, the energy shifting in the O bridging and hydroxyl chemical states are also high in the metal dopant with low oxidation state (see Table S1, Supporting Information). However, for the case of Al, energy shifting in the hydroxyl chemical state is the highest. This infers that the Al has high tendency to form its own oxide, that is, Al_2O_3, which may deteriorate the photocatalytic performance of the TNS system. Raman analysis results further confirm such a variation effect in the host properties when using metal dopants with different oxidation states and the ionic radii. As the Raman results reveal, the main peaks of the host lattice vibration shifted to the higher frequency upon being doped with the

:10.1021/acsomega.8b00109
ACS Omega 2018, 3, 2579−2587

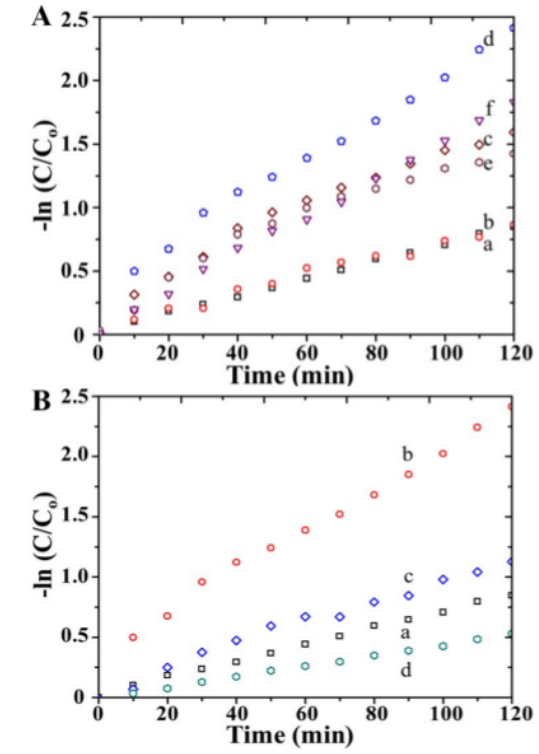

Figure 5. Kinetic rate of photocatalytic degradation of rhodamine B over (A) AgTNS with different Ag concentrations. (a) 0 (pristine TNS), (b) 25, (c) 50, (d) 100, (e) 150, and (f) 200 mM and (B) TNS doped with different metals. (a) Pristine TNS, (b) AgTNS, (c) ZnTNS, and (d) AlTNS.

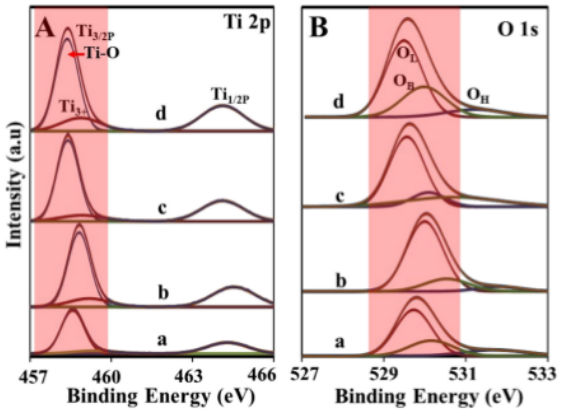

Figure 6. Chemical state binding energy of Ti and O in TNS samples when being doped with different metals. (a) Pristine TNS, (b) AgTNS, (c) ZnTNS, and (d) AlTNS. Shaded region in A and B highlights the Ti and O chemical state binding energy shifting due to the doping process.

metal with the highest shift was shown by the Ag doping. The shifting to the higher frequency domain indicates the improvement in the crystallinity by decreasing the crystal defects. It is also related to the increase of the oxygen vacancy on the material surface. In addition, for the case of Ag doping, the band symmetry (see Eg(1) band) is strongly altered, which reveals the existence of phonon confinement in the lattice presumably because of an immense distortion in the crystal lattice symmetry modifying the O−Ti−O or Ti−O vibration and bending nature. Combination of the high crystallinity degree and immense lattice symmetry distortion in Ag doping may lead to the decrease in the photoelectron and hole recombination and the enhancement of the photogenerated carrier formation, enhancing the photocatalytic performance of the TNS (Figure 7).

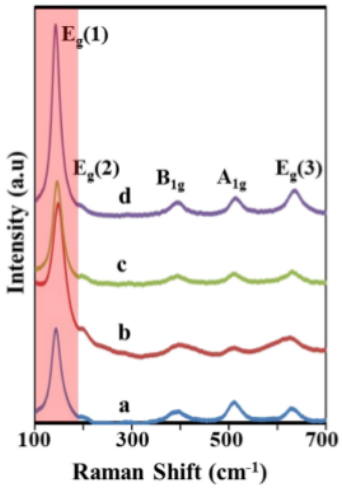

Figure 7. Raman spectra of TNS samples doped with different metals. (a) Pristine TNS, (b) Ag, (c) Zn, and (d) Al. Shaded region indicated Raman peak shifting and peak symmetry modification.

CONCLUSIONS

Hierarchical, porous, and high-energy faceted AgTNS demonstrates high photocatalytic performance in the degradation of the RhB dye with ToN and ToF as high as 94 and 1.57 min^{-1}, respectively, and equivalent to the degradation of 91.1 mmol mg^{-1} W^{-1}. The result also indicates that the AgTNS performance is 2 times higher than the pristine TNS and several order higher compared to Zn- and Al-doped TNS as well as compared to the recently reported result. The main reason for the high photocatalytic performance is due to (i) the improvement of the crystallinity degree of the TNS, (ii) decrease of the defect density and the photogenerated electron and hole recombination, and (iii) increase of the oxygen vacancy upon being doped with the Ag ions. The hierarchical and porous (001) faceted metal-doped TNS should find an extensive application in a wide range of fields, such as dye-sensitized solar cells, photoelectrochemical water splitting, sensors, and so forth, and its performance is predicted to be upgradable by improving their bulk and surface chemistry properties, such as crystallinity and surface refinement.

MATERIALS AND METHOD

Synthesis of the Two-Dimensional AgTNS. Two-dimensional, hierarchical, porous AgTNS or simply called as AgTNS nanosheets were prepared using our previously reported method, namely, liquid phase deposition method

DOI: 10.1021/acsomega.8b00109
ACS Omega 2018, 3, 2579−2587

with a modification.[25] In the normal process, AgTNS was prepared by mixing 1 mL of 100 mM $AgNO_3$, 5 mL of aqueous solution of 0.5 M $(NH_4)_2TiF_6$, and 1 mL of 0.5 M HMT altogether. The solution was then ultrasonicated for 2 min for a better mixing the solution. After that, the mixed solution was kept undisturbed for 5 h in a water bath at a temperature of 90 °C. A white precipitate was obtained from this process and collected via centrifugation at 400 rpm for 15 min. The supernatant was removed using a micropipette, and the white powder precipitate was then transferred to an alumina crucible. The sample was then transferred into the furnace for drying and then annealed at 400 °C for 1 h in air. From this process, anatase AgTNS will be obtained.

To obtain AgTNS with different Ag contents, five different concentrations of $Ag(NO_3)_2$, that is, 25, 50, 100, 150, and 200 mM, were used. The effect of the metal dopant on the photocatalytic performance of the TNS, two more metal dopants, that is, Zn and Al, were used in this study. For the preparation of ZnTNS and AlTNS, the $ZnNO_3{\cdot}xH_2O$ and $Al_2(NO_3)_3{\cdot}9H_2O$ were introduced into the growth solution instead of $AgNO_3$.

AgTNS Characterization. The morphology of AgTNS was characterized using the FESEM technique (Zeiss MERLIN). The crystallinity of the nanosheet sample was analyzed using a S/TEM FEI Tecnai G2 F20 operated at 200 kV acceleration voltage. The elemental composition of AgTNS and its distribution was also analyzed using the same apparatus via the electron energy dispersion technique using Aztech Instruments with an acceleration voltage of 15 kV. The crystal structure and the phase of the AgTNS were characterized using the XRD technique using Bruker D8 with Cu Kα of 1.54 Å with a scan rate of as 2°/min. While the optical properties and the surface chemistry of the samples were characterized by the diffuse reflectance method using a Hitachi U39000-H spectrophotometry system and a XPS Shimadzu XSAM-HS system from Kratos, UK, with monoenergetic X-ray of Al Kα (1486.6 eV), respectively. For these XPS and diffuse reflectance spectroscopy, we used the samples grown on the ITO surface. Measurement of Raman spectroscopy was also carried out on samples prepared on the ITO surface using confocal micro-Raman imaging spectroscopy, Thermo Scientific (model DX2Xi), with 532 nm laser line of Ar^+ laser used as an excitation source.

Photocatalytic Characterization. The photocatalytic property of AgTNS was examined in the photodegradation of rhodamine B under solar light illumination. Solar light simulation 1.5 AM 100 mW cm^{-1} was obtained from an LCT-100 Newport solar simulator, USA. In the photocatalytic degradation study, 10 mL of 10 ppm rhodamine B in aqueous phase was used and prepared in a 30 mL glass vial. AgTNS (1 mg) was then added into the solution and briefly ultrasonicated for 5 s. The solution that contained AgTNS was then put under solar light simulator irradiation. The degradation kinetics of rhodamine B was evaluated by analyzing its optical absorbance in every 10 min of the reaction.

■ ASSOCIATED CONTENT

Supporting Information

The Supporting Information is available free of charge on the ACS Publications website at DOI: 10.1021/acsomega.8b00109.

The detailed morphological, elemental, and chemical state analysis of the Ag-, Zn-, and Al-doped TNS (PDF)

■ AUTHOR INFORMATION

Corresponding Author

*E-mail: akrajas@ukm.edu.my (A.A.U.).

ORCID

Akrajas Ali Umar: 0000-0001-8299-4827

Notes

The authors declare no competing financial interest.

■ ACKNOWLEDGMENTS

The authors thank the Ministry of Higher Education of Malaysia for financial support under the research fundamental grant FRGS/1/2016/STG02/UKM/02/2 and the Universiti Kebangsaan Malaysia under GUP-2016-013 and DIP-2016-022. This work was partly supported by the Nanotechnology Platform Program of the Ministry of Education, Culture, Sports, Science and Technology (MEXT), Japan.

■ REFERENCES

(1) Asahi, R.; Morikawa, T.; Irie, H.; Ohwaki, T. Nitrogen-Doped Titanium Dioxide as Visible-Light-Sensitive Photocatalyst: Designs, Developments, and Prospects. *Chem. Rev.* **2014**, *114*, 9824−9852.

(2) Bourikas, K.; Kordulis, C.; Lycourghiotis, A. Titanium Dioxide (Anatase and Rutile): Surface Chemistry, Liquid−Solid Interface Chemistry, and Scientific Synthesis of Supported Catalysts. *Chem. Rev.* **2014**, *114*, 9754−9823.

(3) Wang, X.; Feng, J.; Bai, Y.; Zhang, Q.; Yin, Y. Synthesis, Properties, and Applications of Hollow Micro-/Nanostructures. *Chem. Rev.* **2016**, *116*, 10983−11060.

(4) Crossland, E. J. W.; Noel, N.; Sivaram, V.; Leijtens, T.; Alexander-Webber, J. A.; Snaith, H. J. Mesoporous TiO2 single crystals delivering enhanced mobility and optoelectronic device performance. *Nature* **2013**, *495*, 215−219.

(5) Fujishima, A.; Honda, K. Electrochemical Photolysis of Water at a Semiconductor Electrode. *Nature* **1972**, *238*, 37−38.

(6) Nozik, A. J. Photoelectrolysis of water using semiconducting TiO_2 crystals. *Nature* **1975**, *257*, 383−386.

(7) Khan, S. U. M.; Al-Shahry, M.; Ingler, W. B. Efficient Photochemical Water Splitting by a Chemically Modified n-TiO_2. *Science* **2002**, *297*, 2243−2245.

(8) Diebold, U. The surface science of titanium dioxide. *Surf. Sci. Rep.* **2003**, *48*, 53−229.

(9) Umar, A. A.; Saad, S. K. M.; Umar, M. I. A.; Rahman, M. Y. A.; Oyama, M. Advances in porous and high-energy (001)-faceted anatase TiO_2 nanostructures. *Opt. Mater.* **2018**, *75*, 390−430.

(10) Al-She'irey, A. Y. A.; Saad, S. K. M.; Umar, A. A.; Rahman, M. Y. A.; Salleh, M. M. (001) faceted-Ga-TiO_2 microtablet synthesis and its organic perovskite sensitized solar cells characterization. *J. Alloys Compd.* **2016**, *674*, 470−476.

(11) Crossland, E. J. W.; Noel, N.; Sivaram, V.; Leijtens, T.; Alexander-Webber, J. A.; Snaith, H. J. Mesoporous TiO_2 single crystals delivering enhanced mobility and optoelectronic device performance. *Nature* **2013**, *495*, 215−219.

(12) Liu, G.; Yang, H. G.; Wang, X.; Cheng, L.; Lu, H.; Wang, L.; Lu, G. Q.; Cheng, H.-M. Enhanced Photoactivity of Oxygen-Deficient Anatase TiO_2 Sheets with Dominant {001} Facets. *J. Phys. Chem. C* **2009**, *113*, 21784−21788.

(13) Roy, N.; Sohn, Y.; Pradhan, D. Synergy of Low-Energy {101} and High-Energy {001} TiO_2 Crystal Facets for Enhanced Photocatalysis. *ACS Nano* **2013**, *7*, 2532−2540.

(14) Zhai, P.; Hsieh, T.-Y.; Yeh, C.-Y.; Reddy, K. S. K.; Hu, C.-C.; Su, J.-H.; Wei, T.-C.; Feng, S.-P. Trifunctional TiO_2 Nanoparticles with Exposed {001} Facets as Additives in Cobalt-Based-Porphyrin Sensitized Solar Cells. *Adv. Funct. Mater.* **2015**, *25*, 6093−6100.

(15) Yang, H. G.; Sun, C. H.; Qiao, S. Z.; Zou, J.; Liu, G.; Smith, S. C.; Cheng, H. M.; Lu, G. Q. Anatase TiO_2 single crystals with a large percentage of reactive facets. *Nature* **2008**, *453*, 638−641.

DOI: 10.1021/acsomega.8b00109
ACS Omega 2018, 3, 2579−2587

(16) Ali Umar, A.; Nafisah, S.; Md Saad, S. K.; Tan, S. T.; Balouch, A.; Mat Salleh, M.; Oyama, M. Poriferous microtablet of anatase TiO_2 growth on an ITO surface for high-efficiency dye-sensitized solar cells. *Sol. Energy Mater. Sol. Cells* **2014**, *122*, 174−182.
(17) Dahlan, D.; Saad, S. K. M.; Berli, A. U.; Bajili, A.; Umar, A. A. Synthesis of two-dimensional nanowall of Cu-Doped TiO_2 and its application as photoanode in DSSCs. *Phys. E* **2017**, *91*, 185−189.
(18) Zhao, X.; Jin, W.; Cai, J.; Ye, J.; Li, Z.; Ma, Y.; Xie, J.; Qi, L. Shape and Size Controlled Synthesis of Uniform Anatase TiO_2 Nanocuboids Enclosed by Active {100} and {001} Facets. *Adv. Funct. Mater.* **2011**, *21*, 3554−3563.
(19) Wu, X.; Chen, Z.; Lu, G. Q. M.; Wang, L. Nanosized Anatase TiO_2 Single Crystals with Tunable Exposed (001) Facets for Enhanced Energy Conversion Efficiency of Dye Sensitized Solar Cells. *Adv. Funct. Mater.* **2011**, *21*, 4167−4172.
(20) Illa, S.; Boppella, R.; Manorama, S. V.; Basak, P. Mesoporous Assembly of Cuboid Anatase Nanocrystals into Hollow Spheres: Realizing Enhanced Photoactivity of High Energy {001} Facets. *J. Phys. Chem. C* **2016**, *120*, 18028−18038.
(21) Xie, S.; Han, X.; Kuang, Q.; Fu, J.; Zhang, L.; Xie, Z.; Zheng, L. Solid state precursor strategy for synthesizing hollow TiO_2 boxes with a high percentage of reactive {001} facets exposed. *Chem. Commun.* **2011**, *47*, 6722−6724.
(22) Cheng, X.-L.; Hu, M.; Huang, R.; Jiang, J.-S. HF-Free Synthesis of Anatase TiO_2 Nanosheets with Largely Exposed and Clean {001} facets and Their Enhanced Rate Performance As Anodes of Lithium-Ion Battery. *ACS Appl. Mater. Interfaces* **2014**, *6*, 19176−19183.
(23) Game, O.; Kumari, T.; Singh, U.; Aravindan, V.; Madhavi, S.; Ogale, S. B. (001) faceted mesoporous anatase TiO_2 microcubes as superior insertion anode in practical Li-ion configuration with $LiMn_2O_4$. *Energy Storage Mater.* **2016**, *3*, 106−112.
(24) Liu, M.; Piao, L.; Lu, W.; Ju, S.; Zhao, L.; Zhou, C.; Li, H.; Wang, W. Flower-like TiO_2 nanostructures with exposed {001} facets: Facile synthesis and enhanced photocatalysis. *Nanoscale* **2010**, *2*, 1115−1117.
(25) Md Saad, S. K.; Umar, A. A1.; Nguyen, H. Q.; Dee, C. F.; Salleh, M. M.; Oyama, M. Porous (001)-faceted Zn-doped anatase TiO_2 nanowalls and their heterogeneous photocatalytic characterization. *RSC Adv.* **2014**, *4*, 57054−57063.
(26) Saad, S. K. M.; Umar, A. A.; Rahman, M. Y. A.; Salleh, M. M. Porous Zn-doped TiO_2 nanowall photoanode: Effect of Zn 2+ concentration on the dye-sensitized solar cell performance. *Appl. Surf. Sci.* **2015**, *353*, 835−842.
(27) Tan, S. T.; AlZayed, N. S.; Lakshminarayana, G.; Naumar, F.; Umar, A. A.; Oyama, M.; Myronchuk, G.; Kityk, I. V. Laser stimulated electrooptics in the Ag−ZnO nanorods. *Phys. E* **2014**, *61*, 23−27.
(28) Tan, S. T.; Ali Umar, A.; Balouch, A.; Nafisah, S.; Yahaya, M.; Yap, C. C.; Mat Salleh, M.; Kityk, I. V.; Oyama, M. Ag−ZnO Nanoreactor Grown on FTO Substrate Exhibiting High Heterogeneous Photocatalytic Efficiency. *ACS Comb. Sci.* **2014**, *16*, 314−320.
(29) Ravishankar, T. N.; Muralikrishna, S.; Nagaraju, G.; Ramakrishnappa, T. Electrochemical detection and photochemical detoxification of hexavalent chromium (Cr (vi)) by Ag doped TiO_2 nanoparticles. *Anal. Methods* **2015**, *7*, 3493−3499.
(30) Zhang, F.; Cheng, Z.; Kang, L.; Cui, L.; Liu, W.; Xu, X.; Hou, G.; Yang, H. A novel preparation of Ag-doped TiO_2 nanofibers with enhanced stability of photocatalytic activity. *RSC Adv.* **2015**, *5*, 32088−32091.
(31) Kityk, I. V.; Umar, A. A.; Oyama, M. Circularly polarized light-induced electrogyration in the Au nanoparticles on the ITO. *Phys. E* **2005**, *27*, 420−426.
(32) Kityk, I. V.; Plucinski, K. J.; Ebothé, J.; Umar, A. A.; Oyama, M. Control of the plasmon absorption of gold nanoparticles with a two-color excitation. *J. Appl. Phys.* **2005**, *98*, 084304.
(33) Kityk, I. V.; Ebothé, J.; Fuks-Janczarek, I.; Umar, A. A.; Kobayashi, K.; Oyama, M.; Sahraoui, B. Nonlinear optical properties of Au nanoparticles on indium-tin oxide substrate. *Nanotechnology* **2005**, *16*, 1687−1692.
(34) Ozga, K.; Oyama, M.; Szota, M.; Nabiałek, M.; Kityk, I. V.; Ślęzak, A.; Umar, A. A.; Nouneh, K. Photoinduced absorption of Ag nanoparticles deposited on ITO substrate. *J. Alloys Compd.* **2011**, *509*, S424−S426.
(35) Shah, A. A.; Umar, A. A.; Salleh, M. M. Efficient quantum capacitance enhancement in DSSC by gold nanoparticles plasmonic effect. *Electrochim. Acta* **2016**, *195*, 134−142.
(36) Sahoo, S. R.; Ramacharyulu, P. V. R. K.; Ke, S.-C. Impact of Nonideal Nanoparticles on X-ray Photoelectron Spectroscopic Quantitation: An Investigation Using Simulation and Modeling of Gold Nanoparticles. *Anal. Chem.* **2018**, *90*, 1621−1627.
(37) Ohsaka, T.; Izumi, F.; Fujiki, Y. Raman spectrum of anatase, TiO_2. *J. Raman Spectrosc.* **1978**, *7*, 321−324.
(38) Zhang, W. F.; He, Y. L.; Zhang, M. S.; Yin, Z.; Chen, Q. Raman scattering study on anatase TiO_2 nanocrystals. *J. Phys. D: Appl. Phys.* **2000**, *33*, 912−916.
(39) Šćepanović, M. J.; Grujić-Brojčin, M.; Dohčević-Mitrović, Z. D.; Popović, Z. V. Characterization of anatase TiO_2 nanopowder by variable-temperature Raman spectroscopy. *Sci. Sintering* **2009**, *41*, 67−73.
(40) Long, L.-L.; Zhang, A.-Y.; Yang, J.; Zhang, X.; Yu, H.-Q. A green approach for preparing doped TiO_2 single crystals. *ACS Appl. Mater. Interfaces* **2014**, *6*, 16712−16720.
(41) Santra, A. K.; Yang, F.; Goodman, D. W. The growth of Ag−Au bimetallic nanoparticles on TiO_2 (110). *Surf. Sci.* **2004**, *548*, 324−332.
(42) Li, W.; Li, D.; Meng, S.; Chen, W.; Fu, X.; Shao, Y. Novel approach to enhance photosensitized degradation of rhodamine B under visible light irradiation by the $Zn_xCd_{1-x}S/TiO_2$ nanocomposites. *Environ. Sci. Technol.* **2011**, *45*, 2987−2993.
(43) Cheng, X.; Yu, X.; Xing, Z. Enhanced photoelectric property and visible activity of nitrogen doped TiO_2 synthesized from different nitrogen dopants. *Appl. Surf. Sci.* **2013**, *268*, 204−208.
(44) Ali, S. M. Y. M. M.; Sandhya, K. One step solvothermal synthesis of ultra-fine N-doped TiO_2 with enhanced visible light catalytic properties. *RSC Adv.* **2016**, *6*, 60522−60529.
(45) Kasinathan, K.; Kennedy, J.; Elayaperumal, M.; Henini, M.; Malik, M. Photodegradation of organic pollutants RhB dye using UV simulated sunlight on ceria based TiO_2 nanomaterials for antibacterial applications. *Sci. Rep.* **2016**, *6*, 1−12.
(46) Deng, Y.; Tang, L.; Zeng, G.; Dong, H.; Yan, M.; Wang, J.; Hu, W.; Wang, J.; Zhou, Y.; Tang, J. Enhanced visible light photocatalytic performance of polyaniline modified mesoporous single crystal TiO_2 microsphere. *Appl. Surf. Sci.* **2016**, *387*, 882−893.
(47) Guo, C.; Xu, J.; He, Y.; Zhang, Y.; Wang, Y. Photodegradation of rhodamine B and methyl orange over one-dimensional TiO_2 catalysts under simulated solar irradiation. *Appl. Surf. Sci.* **2011**, *257*, 3798−3803.
(48) Javaid, S.; Farrukh, M. A.; Muneer, I.; Shahid, M.; Khaleeq-Ur-Rahman, M.; Umar, A. A. Influence of optical band gap and particle size on the catalytic properties of Sm/SnO_2-TiO_2 nanoparticles. *Superlattices Microstruct.* **2015**, *82*, 234−247.
(49) Agyeman, D. A.; Song, K.; Kang, S. H.; Jo, M. R.; Cho, E.; Kang, Y.-M. An improved catalytic effect of nitrogen-doped TiO_2 nanofibers for rechargeable Li-O_2 batteries; the role of oxidation states and vacancies on the surface. *J. Mater. Chem. A* **2015**, *3*, 22557−22563.

DOI: 10.1021/acsomega.8b00109
ACS Omega 2018, 3, 2579−2587

Karya#5 Plagiasi

ORIGINALITY REPORT

7%	4%	8%	%
SIMILARITY INDEX	INTERNET SOURCES	PUBLICATIONS	STUDENT PAPERS

PRIMARY SOURCES

1	Akrajas Ali Umar, Siti Khatijah Md Saad, Marjoni Imamora Ali Umar, Mohd Yusri Abd Rahman, Munetaka Oyama. "Advances in porous and high-energy (001)-faceted anatase TiO 2 nanostructures", Optical Materials, 2018 Publication	2%
2	Dahyunir Dahlan, Muhamad Adam Ramli, Khudbatul Fiqrian, Siti Khatijah Md Saad, Munetaka Oyama, Akrajas Ali Umar. "Thermal impact on (001) faceted anatase TiO2 microtablets and nanowalls's lattices and its effect on the photon to current conversion efficiency", Journal of Physics and Chemistry of Solids, 2019 Publication	1%
3	Kiran Gupta, R P Singh, Ashutosh Pandey, Anjana Pandey. " Correction: Photocatalytic antibacterial performance of TiO and Ag-doped TiO against and ", Beilstein Journal of Nanotechnology, 2020 Publication	1%

4	E.R. Mawarnis, A.A. Umar. "Fibrous bimetallic silver palladium and ruthenium palladium nanocrystals exhibit an exceptionally high active catalytic process in acetone hydrogenation", Materials Today Chemistry, 2019 Publication	1%
5	www.science.gov Internet Source	1%
6	ir.uiowa.edu Internet Source	1%
7	Siti Khatijah Md Saad, Akrajas Ali Umar, Mohd. Yusri Abd. Rahman, Muhamad Mat Salleh. "Porous Zn-doped TiO2 nanowall photoanode: Effect of Zn2+ concentration on the dye-sensitized solar cell performance", Applied Surface Science, 2015 Publication	1%

Exclude quotes	On	Exclude matches	< 1%
Exclude bibliography	On		